Thermalization of Nuclear Spins in Lanthanide Molecular Magnets

Gheorghe Taran, Edgar Bonet, Eufemio Moreno-Pineda,* Mario Ruben,* and Wolfgang Wernsdorfer*

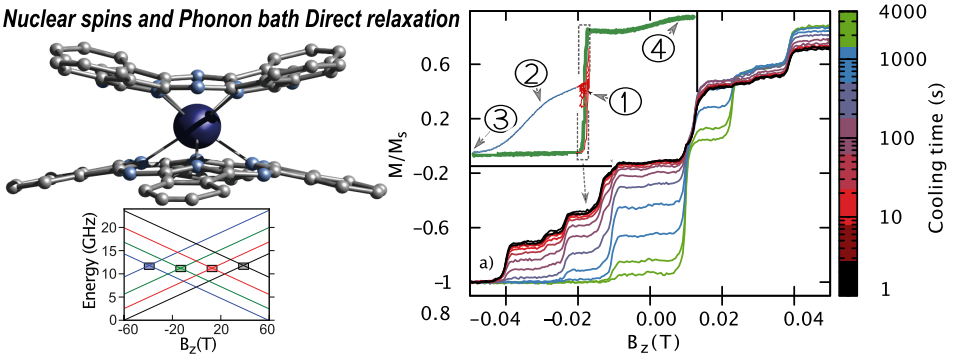

ABSTRACT: Single-molecule magnets (SMMs) distinguish themselves in the field of quantum magnetism through the ability to combine fundamental research with promising applications. The evolution of quantum spintronics in the last decade exemplifies the potential held by molecular-based quantum devices. Notably, the readout and manipulation of the nuclear spin states embedded in a lanthanide-based SMM hybrid device were employed in proof of principle studies of quantum computation at the single-molecule level. In the quest for further understanding of the relaxation behavior in SMMs for their integration in novel applications, herein, we study the relaxation dynamics of the ^{159}Tb nuclear spins in a diluted molecular crystal employing the recently acquired understanding of the nonadiabatic dynamics of $TbPc_2$ molecules. Through numerical simulation, we find that phonon-modulated hyperfine interaction opens a direct relaxation channel between the nuclear spins and the phonon bath. The mechanism is of potential importance for the theory of spin bath and the relaxation dynamics of the molecular spins.

INTRODUCTION

The advancement toward industrially viable quantum technologies, such as quantum computing and nanoscale magnetometry, depends largely on our ability to control the immediate environment of a system of interacting quantum objects (qubits).[1,2] The main objective is to preserve coherence during external manipulations and, thus, exploit intrinsic quantum properties such as interference[3] and entanglement.[4] Depending on their nature and coupling strength, most environmental degrees of freedom interacting with the qubit can be mapped either into a bosonic bath, for nonlocal, weak interactions, or to a spin bath, in the case of localized, strong interactions.[5] The latter case is especially important, as it can induce decoherence even in the $T \rightarrow 0$ limit, that is, the dephasing is not accompanied by dissipative processes. Consequently, the complex problem of a central quantum system coupled to localized environmental excitations, for example, nuclear spins or paramagnetic centers, is pivotal in mesoscopic quantum physics.[6,7]

Among experimental implementations of interacting quantum systems (e.g., NV centers in diamond,[8] nanomagnets,[9,10] SQUIDs,[3] and impurities in silicon[8]), molecular magnets exemplify particularly well the intimate relationship that exists between the manifested quantum phenomenology (e.g., quantum tunneling of magnetization (QTM),[11] spin parity effects,[12] Rabi oscillations[13]), and the spin bath. After the bistability of Mn_{12}-ac[14] was first experimentally evidenced—an event that marked the birth of the field of molecular magnetism—the breakthrough discoveries of both phonon-assisted and ground-state quantum tunneling[15] greatly boosted the interest in these systems. Theoretical conundrums to explain the observed dynamics were resolved by carefully considering the effect of the environmental interactions (both spin−phonon and spin−spin couplings) and thus contributed significantly to the development of the theory of the spin bath.[16] Molecular magnets also proved to be ideal systems for testing the predictions made by the constructed theory. Therefore, both the influence of the isotopic composition, through variation of the hyperfine interaction on the relaxation

rate,[17] and the peculiar square root law for the relaxation at low temperatures and short times were promptly verified.[18] The strong correlations between the dynamics of the spin bath and the relaxation of the molecular spin were also evidenced by measuring directly the nuclear spins through resonant techniques.[19] Both the longitudinal and transverse relaxation times were linked directly to the electronic spin dynamics,[20] proving that nuclear spins can serve as microscopic probes for the molecular spin.[21] The theory of the spin bath was also successfully applied in the study of the decoherence in crystals of molecular magnets,[22,23] paving the way for molecular optimization for quantum information processing nanodevices.

Most of the experimental and theoretical investigations into the subject of spin bath were carried out employing transition-metal ion compounds as model systems (e.g., Mn_{12}-ac and Fe_8) because these were the first discovered SMMs and, for a long time, remained the best-understood compounds.[24] However, the last decade saw the rise of molecular complexes that employ lanthanide ions as magnetic centers, arguably the most promising SMMs. Recent achievements include the observation of magnetic bistability of a Dy^{3+} complex at temperatures well above liquid nitrogen[25−27] and the implementation of the quantum Grover algorithm at the single-molecule level.[28]

Unquenched orbital angular momentum, large single-ion anisotropy, and strong hyperfine interaction are just some characteristics that distinguish lanthanide complexes in the field of molecular magnetism.[29] For example, it was shown that the nature of the strong interaction between the electronic shell of the lanthanide ion and its own nuclear spin has strong repercussions on the tunneling dynamics.[7,30,31] Furthermore, the non-zero orbital momentum brings upfront the spin−phonon interaction. Thus, even in the range where the dynamics is temperature-independent, the phonon bath can no longer be ignored. Despite these observations, the quantum dynamics of lanthanide SMMs in the framework of the spin bath theory is a subject largely unexplored.

In the theoretical endeavor undertaken to improve the understanding of the displayed dynamics, the properties of the lanthanide molecular complex immersed in a bath of both bosonic and spin nature have to be considered. The main difficulties arise when the dynamics of the bath is strongly coupled to the dynamics of the central spin, as the effect of the environment cannot be treated perturbatively. However, the analysis of the properties of the spin bath when the molecular spins are static is an important first step.

In this paper, a piece of the puzzle is studied as the thermalization of the $^{159}Tb^{3+}$ nuclear spins in a crystal of prototypical $[TbPc_2]^-$ molecule is investigated. For this study, the prototypal $[TbPc_2]^-$ complex was chosen as a model system as the acquired understanding on the dynamics of its magnetization facilitated the development of a readout technique for the population of the hyperfine states.[32−36] Hence, in this work, we set off by analyzing the sub-kelvin magnetization dynamics of $[TbPc_2]^-$ in a varying magnetic field and its link to the distribution of the nuclear spins. Thenceforth, the time evolution of the population of the hyperfine states, obtained by fitting the magnetization curves, is evaluated in the framework of a Markovian master equation that allows the interpretation of the dynamics in terms of spin−phonon relaxation rates. Finally, by evaluating the temperature dependence of the relaxation process, the main mechanism responsible for the thermalization of the nuclear spins is identified. A direct relaxation process, that involves phonon modulation of the hyperfine interaction, was found sufficient to explain the magnitude of the determined relaxation rates.

RESULTS

$TbPc_2$ Single-Molecule Magnet. μSQUID measurements were conducted on micrometer-sized crystals containing $TBA[TbPc_2]$ molecules (Figure 1a) diluted in an isostructural

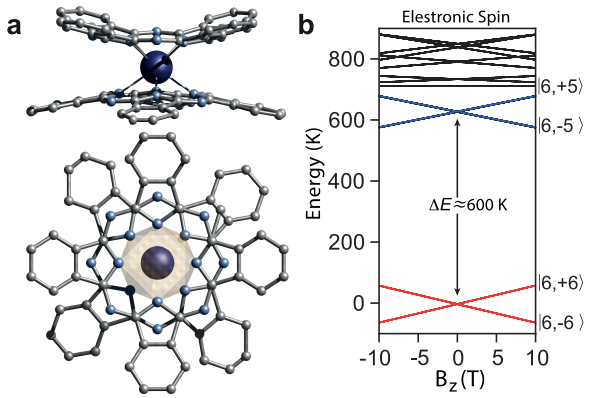

Figure 1. (a) Molecular structure of the $[TbPc_2]^-$ complex. (b) Electronic energy manifold for the $[TbPc_2]^-$ complex, showcasing the separation of the ground doublet and first excited doublet states.

diamagnetic matrix ($TBA[YPc_2]$). The studied crystals correspond to the same batch of those studied in 2005[30] and contain a 2% nominal ratio (i.e., $TBA[Tb_{0.02}Y_{0.98}Pc_2]$). The concentration of the doped sample corresponded to the reactant ratio and was not experimentally verified. The dilution controls the dipolar interaction between the molecular spins and, consequently, is used to reduce the probability of the collective effects. Consequently, on the one hand, a diluted sample shows a well-resolved hyperfine structure, and on the other, its dynamics can be understood in terms of the properties of an ensemble of noninteracting molecular spins.

The $[TbPc_2]^-$ molecule features a Tb^{3+} ion sandwiched between two phthalocyanine planes in a square antiprismatic symmetry (D_{4d}). The magnetic properties of the compound are dominated by the single-ion anisotropy of the Tb^{3+} ion that gives a spin ground state $J = 6$ and by the uniaxial character of the ligand field interaction that further splits the $2J + 1$ degenerate eigenstates. As a result of the above interactions, in zero external field, a ground-state doublet ($m_J = \pm 6$), well separated from the first excited doublet ($m'_J = \pm 5$) by about 600 K,[37] is obtained (Figure 1b). Hence, at temperatures much lower than the zero-field splitting, the molecular spin $J = 6$ can be described as an effective spin 1/2 with an effective g-value, $g_{\text{eff}} = 18$. Under an external field parallel to the anisotropy z-axis, the effective two-level Hamiltonian describing the electronic states can be written as

$$\mathcal{H}_e = \frac{g_{\text{eff}}}{2}\mu_B B_z \sigma_z + \frac{\Delta}{2}\sigma_x \tag{1}$$

where the first term represents the longitudinal Zeeman interaction and the second one models the nonaxial ligand field interactions. The tunnel splitting, Δ, was shown to be in the micro-Kelvin range.[38] The $^{159}Tb^{3+}$ nucleus that lies at the heart of the molecule also has a non-zero nuclear spin, $I = 3/2$, which couples to the surrounding electronic shell and further

splits the ground doublet, $m_J = \pm 6$ in a manifold of four levels (zoomed region in Figure 1b). The interaction is modeled by adding a hyperfine and a nuclear quadrupolar contribution to the spin Hamiltonian. Thus, the total Hamiltonian is

$$\mathcal{H}_{TbPc_2} = \mathcal{H}_e + A_{hyp}|m_J|(\boldsymbol{\sigma}\cdot\mathbf{I}) + \mathbf{I}\hat{P}_{quad}\mathbf{I} \quad (2)$$

The isotropic hyperfine interaction, $A_{hyp}|m_J|(\boldsymbol{\sigma}\cdot\mathbf{I})$, has three components: the Fermi contact interaction, the paramagnetic spin−orbit contribution, and the dipole−dipole interaction resulting in the hyperfine constant $A_{hyp} = 26.7$ mK. Because $I > 1/2$, the $^{159}Tb^{3+}$ nucleus has a quadrupolar moment that couples to the electric field gradient through $\mathbf{I}\hat{P}_{quad}\mathbf{I}$, with the dominant term being the axial component with magnitude $P_{quad} = 17$ mK. The tensorial nature of $\hat{P}_{quad}$ reflects the nonaxial character (with respect to the easy axis of the ligand field) of the quadrupolar interaction, which, together with the $\frac{\Delta}{2}\sigma_x$ term of the electronic Hamiltonian, was shown to be responsible for the observed tunneling dynamics of $[TbPc_2]^-$ in diluted single crystals.[31]

The states are labeled using the electronic and nuclear spin components, $|m_J,m_I\rangle$, with $m_J = \pm 6$ and $m_I = -3/2$ to $3/2$. $\mathcal{H}_{TbPc_2}$ is numerically written in the above basis. Diagonalization of $\mathcal{H}_{TbPc_2}$ in the presence of a magnetic field in the range [−50:50] mT yields the Zeeman diagram shown in Figure 2b. As can be clearly seen, the interaction between the electronic spin and nuclear spin results in the nonequidistant splitting of the energy levels, with energy spacings between consecutive hyperfine states of around 120, 160, and 190 mK. For temperatures comparable to the hyperfine splitting, a nonequilibrium distribution of the population of the hyperfine states is expected to evolve toward the Boltzmann distribution on a time scale determined by the relaxation mechanism(s).

Experiment. In the present study, a μSQUID magnetometer was employed, as it is highly sensitive to the magnetic field generated by the molecular spin moments. To qualitatively understand the link between the magnetization curve ($M(B_z)$) exhibited by the $[TbPc_2]^-$ diluted crystal and the population of the hyperfine states, Figure 2a shows a closer view of the $M(B_z)$ characteristic at 50 mK (ref 30 for details).

When starting with a saturated sample in a large magnetic field applied along the easy axis ($B_z \approx -1.3$ T) and then sweeping the magnetic field, no relaxation is observed until level crossings in the Zeeman diagram are reached (Figure 2b). This ascertains that the temperature is low enough so that the over-barrier relaxation through the interaction with the lattice vibrations is an improbable process (Figures S1−S3). As the first crossing in the Zeeman diagram is reached ($B_z \approx -40$ mT), a relaxation step in the magnetization curve is observed. This bears evidence to resonant quantum tunneling processes induced by the nonaxial interactions. The height of the relaxation step depends both on the tunneling probability and on the population of the levels that form the anticrossing. Thus, if the tunneling probability is known, the population of the hyperfine states can be obtained by fitting the magnetization curves.

As the magnetic field is swept, new steps that correspond to the subsequent level anticrossings are observed. The height of the steps will no longer depend only on the initial population of the hyperfine states but also on the previous tunneling events. It should be noticed that the small relaxation that is seen in between the steps is mainly due to dipolar interactions

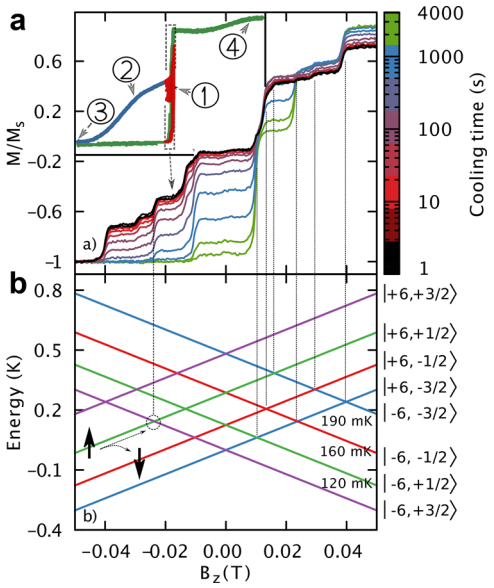

Figure 2. (a) Magnetization curves of a diluted $[TbPc_2]^-$ crystal measured with the μSQUID technique at 50 mK as a function of the cooling time. The sample is kept in $B_z = -1.3$ T (the cooling time is indicated via the color code bar on the right). The inset shows the μSQUID loops between ±1.3 T, while the gray rectangle highlights the zoomed region shown in (a). The full procedure to measure the magnetization curves is detailed in the inset as follows: (1) initialization of the sample by sweeping through the zero-field resonances multiple times until the $M = 0$ state is reached (a hot state is reached); (2) the sample is saturated with $B_z = -1.3$ T; (3) B_z is kept constant, giving the nuclear spins certain time to thermalize; and (4) the hyperfine populations are read out by inverting the magnetization while measuring $M(B_z)$. (b) Hyperfine structure of the ground doublet, $m_J = \pm 6$, as a function of the applied longitudinal field, obtained after numerical diagonalization of the Hamiltonian (2). The large black arrows illustrate how the ^{159}Tb transitions from the state $|+6, +1/2\rangle$ to the state $|+6, -1/2\rangle$ during the thermalization process. These transitions are observed in the magnetization curve as a decrease in the magnitude of the relaxation step.

in the crystal (both of electronic and hyperfine origin) that broaden the resonance. Besides QTM events that occur close to zero field, the hysteresis curve also displays a broad step at higher applied fields, which is due to a direct spin−phonon relaxation process.[39−41] This is a common characteristic of lanthanide SMMs, which is the result of the unquenched orbital angular momentum.

The experimental protocol used to evidence and investigate the thermalization of $^{159}Tb^{3+}$ nuclear spins is shown in the inset of Figure 2a. In order to start with a reproducible initial state, the zero-field resonances are swept repeatedly back and forth between −0.06 and +0.06 mT in order to induce transitions between the hyperfine states. The sample is demagnetized because the probability for the molecular spins to make a transition from $m_J = -6$ to +6 is equal to the probability of the reversed process. Hence, the nuclear spin population reaches an effective temperature, as determined by the Boltzmann distribution,[38] much higher than the cryostat temperature, since the time scale of the nuclear spin thermalization is much longer compared to the time induced by the tunneling transitions. The sample is then saturated in a high longitudinal magnetic field ($B_z = -1.3$ T). During this stage, the molecular spins are polarized, that is, all of the molecules will be in the same $m_J = +6$, while the nuclear spin

population remains out of equilibrium. The sample is maintained polarized in $B_z = -1.3$ T for a certain time named the cooling time (t_c). During this cooling time, the population of the $^{159}Tb^{3+}$ nuclear spins are allowed to evolve toward thermal equilibrium. The final step is to read out the nuclear spin states by inverting the applied field while measuring the $M(B_z)$ curve. Figure 2a shows a zoom of the measured magnetization curves for increasingly larger cooling times. It can be seen that the steps corresponding to excited hyperfine states ($m_J = +6$, $m_I > -3/2$) for $B_z < 0$ T gradually diminish and then disappear as the system evolves toward thermal equilibrium.

Theoretical Analysis. The principles underlying the quantitative analysis of $M(B_z)$ characteristics were already exposed when investigating the Landau–Zener dynamics in $[TbPc_2]^-$ diluted crystals.[38] In the aforementioned study, the knowledge about the equilibrium Boltzmann distribution was used to fit the magnetization curve and to infer the tunneling probability, while in the current study, the acquired understanding is employed to obtain the fractional population of the nuclear spin states as a function of the cooling time (see the Supporting Information).

Figure 3 shows the evolution of the population of the hyperfine states as a function of t_c obtained from the fit of the

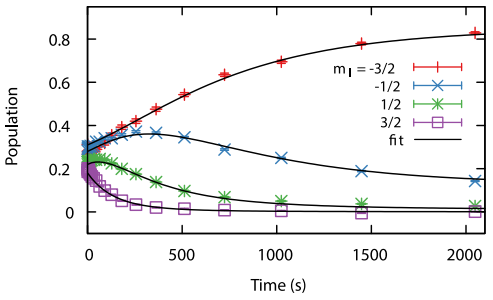

Figure 3. Evolution toward thermal equilibrium of the populations of the hyperfine levels at 50 mK evaluated in the context of the master eq 3. The fitting parameters are the de-excitation transition rates, γ_m.

$M(B_z)$ characteristics. It can be seen that the initial state corresponds to a strongly nonequilibrium configuration, the populations of the hyperfine states being close to equal. Also, at 50 mK, the relaxation is rather slow, as the equilibrium Boltzmann distribution is reached on the time scale of thousands of seconds. Another observation regards the population of $|+6, -1/2\rangle$ state (and to some degree of $|+6, +1/2\rangle$), which shows small changes during the initial phase of the thermalization process. This suggests that the relaxation process that brings the system to the equilibrium Boltzmann distribution follows the selection rule: $\Delta m_I = \pm 1$.

To obtain further insight into the relaxation process(es) that dominates the observed dynamics, the thermalization of the nuclear spins is modeled using a standard master equation for a memoryless, Markovian evolution.

$$\frac{d}{dt}n(m;\,t) = \sum_{q=m\pm1} [\gamma_q^m n(q;\,t) - \gamma_m^q n(m;\,t)] \tag{3}$$

where n represents the fractional populations of the hyperfine levels; m and q denote the hyperfine states and take values between $-3/2$ to $3/2$. The γ_q^m coefficients denote the transition rate from the state $|+6, q\rangle$ to the state $|+6, m\rangle$. The relaxation rates γ_q^m obey the detailed balance condition: $\gamma_m^{m'}/\gamma_{m'}^m = \exp(\beta(E(m) - E(m')))$ with $\beta = 1/(k_B T)$. The sum in (3) is taken only over the nearest-neighbor levels to reflect the above selection rule and reduce the number of fitting parameters. The fit of the master eq 3 to the thermalization process at 50 mK is shown as black lines in Figure 3, with the three de-excitation rates γ_m^{m-1} (from now on denoted simply as γ_m) as the only fitting parameters.

In order to identify the relaxation processes, the above-presented analysis was repeated for temperatures up to 300 mK, where the model for the magnetization curve starts to break down, and the estimation of the population of the hyperfine states is no longer accurate (see Figure S6). Figure 4

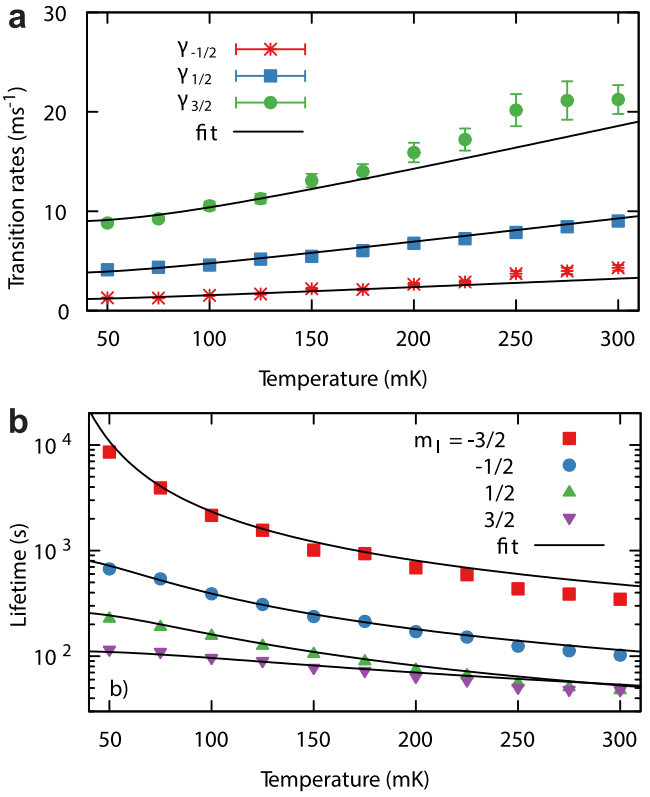

Figure 4. (a) Temperature dependence of the relaxation rates fitted to a direct relaxation process characterized by a spontaneous and induced component and given by eq 4. (b) Temperature dependence of the lifetime of the hyperfine levels computed by using $1/\tau_m = (\gamma_m^{m-1} + \gamma_m^{m+1})$. The continuous lines denote the evaluation of the level lifetimes using eq 4. In the $T \to 0$ limit, the lifetime of the ground state, $|+6, -3/2\rangle$, becomes infinite, while τ_m of the excited states are mainly determined by the spontaneous emission process.

shows the obtained temperature dependence of the relaxation rates and the corresponding lifetimes of the hyperfine levels: $1/\tau_m = (\gamma_m^{m-1} + \gamma_m^{m+1})$. The transition rates increase with the spacing between the hyperfine levels, and for temperatures roughly smaller than 100 mK, the relaxation process becomes temperature-independent. This suggests that the transition rates are determined by the sum of a spontaneous and an induced process. Thus, considering a pair of adjacent hyperfine levels $|+6, m\rangle$ and $|+6, m-1\rangle$ separated in energy by ΔE_m, the transition rate γ_m can be expressed as

$$\gamma_m = \mathcal{F}(\Delta E_m)\frac{\exp(\beta\Delta E_m)}{\exp(\beta\Delta E_m) - 1} \tag{4}$$

The fit curves are shown in Figure 4 as black lines with the fit parameter $\mathcal{F}(\Delta E_m)$ = 1.09, 3.81, and 8.86 ($\times 10^{-3}$ s^{-1}) for the three de-excitation transitions, γ_m, with $m = -1/2$, $+1/2$, and $+3/2$. The expression (4) works especially well at low temperatures ($T \leq 200$ mK), while the deviations occurring at higher temperatures suggest that the inclusion of higher-order processes (e.g., Raman or Orbach mechanisms) may play a role in the relaxation dynamics. At this point, the limited temperature range of our experimental setup precludes the extraction of more details concerning high-temperature relaxation processes.

In order to validate $\mathcal{F}(\Delta E_m)$, the coupling mechanism between the nuclear spins and phonon bath should be considered. The electronic shell of the Tb^{3+} ion couples to the lattice vibrations through the ligand field interaction, while the link between the electronic configuration and the $^{159}Tb^{3+}$ nuclear spins is made through the hyperfine (mainly the spin–orbit term) and quadrupolar interactions. Hence, the transition rates induced by the phonon modulation of the nuclear spin Hamiltonian are computed (refs 42, 43 see the Supporting Information):

$$\mathcal{F}(\Delta E_m) = \frac{m_J^2 \delta A_{hyp}^2 \Delta E_m^3}{6\pi\hbar^4 \rho c^5}(I(I+1) - m(m-1)) \quad (5)$$

where ρ is the crystal density and c is the sound velocity. To our knowledge, measurements of both ρ and c in $[TbPc_2]^-$ crystals were not reported so far; thus, these are taken as free parameters. Especially, variations in the sound velocity will have a big impact on the relaxation rate as it enters in eq 5 to the fifth power. Also, the Debye model (a linear dispersion for the acoustic phonon modes) used in the derivation of eq 5 is an over-simplification. However, due to the lack of ρ and the details on the lattice modes, a rough estimation of the order of magnitude of the relaxation rates is attempted. Thus, by using eq 4 and 5 for the evaluation of $\gamma_{-1/2}$ at 50 mK, the following value is obtained: $\rho c^5 \approx 3.5 \times 10^{19}$ kg·m^2/s^5, while by setting a sensible value for ρ = 1500 kg/m^3, a c = 1877 m/s is found, which is a reasonable enough value (for example, c = 1450 m/s was used to explain phonon-assisted tunneling in Mn_{12}-ac[43]) to confirm the proposed mechanism for the thermalization process. Note that the modulation of the quadrupolar interactions will open additional relaxation pathways. However, as the hyperfine interaction is the dominant nuclear electronic interaction, its modulation leads to faster relaxation rates and thus will dominate the relaxation process. Furthermore, considering the energies involved and the validity of our model ($T \leq 200$ mK), the most probable phonons playing a role in the direct relaxation process are acoustic phonons.[44−46]

The identified direct relaxation channel between the ^{159}Tb nuclear spins and the phonon bath is an important finding for the relaxation of a nuclear spin embedded in a molecular complex. For example, measurements on ^{55}Mn nuclear spins at the core of Mn_{12}-ac SMM were employed to test the predictions of the spin bath theory for the dynamics of molecular spin–nuclear bath coupled system.[47] Most of the observed phenomenologies, with the exception of ^{55}Mn thermalization, were successfully explained. It was then suggested that ^{55}Mn nuclear spins thermalize through the quantum dynamics of the molecular spins because the spin–lattice interactions were found inefficient to explain the measured relaxation rates. However, no theoretical solution to this problem was found. The relaxation mechanism that we evidence for ^{159}Tb is not efficient in the case of ^{55}Mn nuclear spins because the hyperfine interaction in transition-metal ion compounds is around one order of magnitude smaller. Another interesting example to consider is the spin lattice relaxation of ^{159}Tb in a single $TbPc_2$ molecule spin-transistor geometry.[32] The relaxation process, with a characteristic time of tens of seconds, was found to be dominated by the interaction with the electrons that tunnel through the molecular quantum dot. The comparison between the two experiments, which share the same molecular complex, placed in very different environments, suggests that the direct relaxation mechanism that we highlight in this work sets the lower limit for the nuclear relaxation rate in potential lanthanide SMM-based spintronics devices. Note that although the spin-transistor experiment concerns with a single molecule, in which the phonon modes are restricted,[40] the readout highly disturbs the dynamics of the system.[32] Additionally, the effect of the nuclear isotopes on the molecular spin relaxation was evidenced when comparing two isotopologue lanthanide dimers.[48] It was shown that the presence of the nuclear spin leads to a significant increase in the relaxation rate at crossover temperatures, that is, when molecular spin tunneling and phonon-assisted transitions occur with comparable rates. We suggest that the missing ingredient for constructing a quantitative explanation of the observed dynamics is the thermal fluctuations of the nuclear spin.

CONCLUSIONS

In conclusion, we have investigated the thermalization of $^{159}Tb^{3+}$ nuclear spins belonging to the archetypical $[TbPc_2]^-$ complex and proven that the relaxation is due to the phonon modulation of the hyperfine interaction.[31] The uncharacteristic, sub-kelvin, phonon-induced hyperfine fluctuations should be especially important in the crossover temperature domain. Through this work, we try to argue that the direct contact of the nuclear spins to the phonon modes in lanthanide compounds is an important feature that has to be considered both in the continuous search for molecular compounds with optimized magnetic properties and fundamental investigations on the spin bath dynamics.[44−46]

AUTHOR INFORMATION

Corresponding Authors

Eufemio Moreno-Pineda − *Depto. de Química-Física, Facultad de Ciencias Naturales, Exactas y Tecnología, Universidad de Panamá, Panamá 0824, Panamá; Grupo de Investigación de Materiales, Facultad de Ciencias Naturales, Exactas y Tecnología, Universidad de Panamá, Panamá 0824, Panamá;* orcid.org/0000-0002-9643-0341; Email: eufemio.moreno@up.ac.pa

Mario Ruben − *Centre Européen de Sciences Quantiques (CESQ) within the Institut de Science et d'Ingénierie Supramoléculaires (ISIS), 67083 Strasbourg, France; Institute of Nanotechnology (INT), Karlsruhe Institute of Technology (KIT), D-76344 Eggenstein-Leopoldshafen, Germany; Institute for Quantum Materials and Technology*

(IQMT), Karlsruhe Institute of Technology (KIT), D-76344 Eggenstein-Leopoldshafen, Germany; Email: mario.ruben@kit.edu

Wolfgang Wernsdorfer − *Physikalisches Institut, Karlsruhe Institute of Technology, D-76131 Karlsruhe, Germany; Institute of Nanotechnology (INT), Karlsruhe Institute of Technology (KIT), D-76344 Eggenstein-Leopoldshafen, Germany; Institute for Quantum Materials and Technology (IQMT), Karlsruhe Institute of Technology (KIT), D-76344 Eggenstein-Leopoldshafen, Germany;* orcid.org/0000-0003-4602-5257; Email: wolfgang.wernsdorfer@kit.edu

Authors

Gheorghe Taran − *Physikalisches Institut, Karlsruhe Institute of Technology, D-76131 Karlsruhe, Germany*

Edgar Bonet − *Néel Institute, CNRS, Grenoble 38042, France*

Author Contributions

W.W. conceived the idea and supervised the project. G.T. and E.B. collected, processed, and simulated the data and interpreted the results with W.W. M.R. and E.M.-P. synthesized and characterized the samples. The manuscript was written by G.T. and E.M.-P. with input from all authors.

Notes

The authors declare no competing financial interest.

ACKNOWLEDGMENTS

The authors acknowledge the DFG-CRC 1573 "4f for Future" and the Karlsruhe Nano Micro Facility (KNMF, www.kit.edu/knmf) for provision of access to instruments at their laboratories. E.M.-P. thanks the Panamanian National System of Investigators (SNI) and SENACYT (project PFID-FID-2021-60) for support. W.W. thanks the A. v. Humboldt Foundation and the ERC grant MoQuOS No. 741276."

REFERENCES

(1) Atzori, M.; Sessoli, R. The Second Quantum Revolution: Role and Challenges of Molecular Chemistry. *J. Am. Chem. Soc.* **2019**, *141*, 11339−11352.

(2) Dowling, J. P.; Milburn, G. J. Quantum Technology: The Second Quantum Revolution. *Philos. Trans. R. Soc., A* **2003**, *361*, 1655−1674.

(3) Fagaly, R. L. Superconducting Quantum Interference Device Instruments and Applications. *Rev. Sci. Instrum.* **2006**, *77*, No. 101101.

(4) Manzalini, A.; Amoretti, M. End-to-End Entanglement Generation Strategies: Capacity Bounds and Impact on Quantum Key Distribution. *Quantum Rep.* **2022**, *4*, 251−263.

(5) Prokof'ev, N. V.; Stamp, P. C. E. Theory of the Spin Bath. *Rep. Prog. Phys.* **2000**, *63*, 669−726.

(6) Yang, W.; Ma, W.-L. L.; Liu, R.-B. B. Quantum Many-Body Theory for Electron Spin Decoherence in Nanoscale Nuclear Spin Baths. *Rep. Prog. Phys.* **2017**, *80*, No. 016001.

(7) Lunghi, A. Toward Exact Predictions of Spin-Phonon Relaxation Times: An Ab Initio Implementation of Open Quantum Systems Theory. *Sci. Adv.* **2022**, *8*, No. eabn7880.

(8) Awschalom, D. D.; Epstein, R.; Hanson, R. The Diamond Age of Spintronics. *Sci. Am.* **2007**, *297*, 84−91.

(9) Moreno-Pineda, E.; Godfrin, C.; Balestro, F.; Wernsdorfer, W.; Ruben, M. Molecular Spin Qudits for Quantum Algorithms. *Chem. Soc. Rev.* **2018**, *47*, 501−513.

(10) Gaita-Ariño, A.; Luis, F.; Hill, S.; Coronado, E. Molecular Spins for Quantum Computation. *Nat. Chem.* **2019**, *11*, 301−309.

(11) Friedman, J. R.; Sarachik, M. P.; Tejada, J.; Ziolo, R. Macroscopic Measurement of Resonant Magnetization Tunneling in High-Spin Molecules. *Phys. Rev. Lett.* **1996**, *76*, 3830−3833.

(12) Wernsdorfer, W.; Bhaduri, S.; Boskovic, C.; Christou, G.; Hendrickson, D. N. Spin-Parity Dependent Tunneling of Magnetization in Single-Molecule Magnets. *Phys. Rev. B* **2002**, *65*, No. 180403.

(13) Bertaina, S.; Gambarelli, S.; Mitra, T.; Tsukerblat, B.; Müller, A.; Barbara, B. Quantum Oscillations in a Molecular Magnet. *Nature* **2008**, *453*, 203−206.

(14) Sessoli, R.; Gatteschi, D.; Tsai, H. L.; Hendrickson, D. N.; Schake, A. R.; Wang, S.; Vincent, J. B.; Christou, G.; Folting, K. High-Spin Molecules: [Mn12O12(O2CR)16(H2O)4]. *J. Am. Chem. Soc.* **1993**, *115*, 1804−1816.

(15) Sangregorio, C.; Ohm, T.; Paulsen, C.; Sessoli, R.; Gatteschi, D. Quantum Tunneling of the Magnetization in an Iron Cluster Nanomagnet. *Phys. Rev. Lett.* **1997**, *78*, 4645−4648.

(16) Prokof'ev, N. V.; Stamp, P. C. E. E. Low-Temperature Quantum Relaxation in a System of Magnetic Nanomolecules. *Phys. Rev. Lett.* **1998**, *80*, 5794−5797.

(17) Wernsdorfer, W.; Caneschi, A.; Sessoli, R.; Gatteschi, D.; Cornia, A.; Villar, V.; Paulsen, C. Effects of Nuclear Spins on the Quantum Relaxation of the Magnetization for the Molecular Nanomagnet Fe8. *Phys. Rev. Lett.* **2000**, *84*, 2965−2968.

(18) Wernsdorfer, W.; Sessoli, R.; Gatteschi, D. Nuclear-Spin-Driven Resonant Tunnelling of Magnetisation in Mn 12 Acetate. *Europhys. Lett.* **1999**, *47*, No. 254.

(19) Furukawa, Y.; Watanabe, K.; Kumagai, K.; Borsa, F.; Gatteschi, D. Magnetic Structure and Spin Dynamics of the Ground State of the Molecular Cluster Mn12O12 Acetate Studied by 55Mn NMR. *Phys. Rev. B* **2001**, *64*, 1004401−1044017.

(20) Morello, A.; Bakharev, O. N.; Brom, H. B.; Sessoli, R.; de Jongh, L. J. Nuclear Spin Dynamics in the Quantum Regime of a Single-Molecule Magnet. *Phys. Rev. Lett.* **2004**, *93*, No. 197202.

(21) Jang, Z. H.; Lascialfari, A.; Borsa, F.; Gatteschi, D. Measurement of the Relaxation Rate of the Magnetization in Mn12O12-Acetate Using Proton NMR Echo. *Phys. Rev. Lett.* **2000**, *84*, 2977−2980.

(22) Takahashi, S.; van Tol, J.; Beedle, C. C.; Hendrickson, D. N.; Brunel, L. C.; Sherwin, M. S. Coherent Manipulation and Decoherence of S=10 Single-Molecule Magnets. *Phys. Rev. Lett.* **2009**, *102*, 1−4.

(23) Takahashi, S.; Tupitsyn, I. S.; van Tol, J.; Beedle, C. C.; Hendrickson, D. N.; Stamp, P. C. E. E. Decoherence in Crystals of Quantum Molecular Magnets. *Nature* **2011**, *476*, 76−79.

(24) Gatteschi, D.; Sessoli, R. Quantum Tunneling of Magnetization and Related Phenomena in Molecular Materials. *Angew. Chem., Int. Ed.* **2003**, *42*, 268−297.

(25) Goodwin, C. A. P.; Ortu, F.; Reta, D.; Chilton, N. F.; Mills, D. P. Molecular Magnetic Hysteresis at 60 Kelvin in Dysprosocenium. *Nature* **2017**, *548*, 439−442.

(26) Gould, C. A.; McClain, K. R.; Reta, D.; Kragskow, J. G. C.; Marchiori, D. A.; Lachman, E.; Choi, E.; Analytis, J. G.; Britt, R. D.; Chilton, N. F.; Harvey, B. G.; Long, J. R. Ultrahard Magnetism from Mixed-Valence Dilanthanide Complexes with Metal-Metal Bonding. *Science* **2022**, *375*, 198−202.

(27) Guo, F. S.; Day, B. M.; Chen, Y. C.; Tong, M. L.; Mansikkamäki, A.; Layfield, R. A. Magnetic Hysteresis up to 80 Kelvin in a Dysprosium Metallocene Single-Molecule Magnet. *Science* **2018**, *362*, 1400−1403.

(28) Godfrin, C.; Ferhat, A.; Ballou, R.; Klyatskaya, S.; Ruben, M.; Wernsdorfer, W.; Balestro, F. Operating Quantum States in Single Magnetic Molecules: Implementation of Grover's Quantum Algorithm. *Phys. Rev. Lett.* **2017**, *119*, No. 187702.

(29) Woodruff, D. N.; Winpenny, R. E. P.; Layfield, R. A. Lanthanide Single-Molecule Magnets. *Chem. Rev.* **2013**, *113*, 5110−5148.

(30) Ishikawa, N.; Sugita, M.; Wernsdorfer, W. Quantum Tunneling of Magnetization in Lanthanide Single-Molecule Magnets: Bis-

(Phthalocyaninato)Terbium and Bis(Phthalocyaninato)Dysprosium Anions. *Angew. Chem., Int. Ed.* **2005**, *44*, 2931−2935.
(31) Taran, G.; Bonet, E.; Wernsdorfer, W. The Role of the Quadrupolar Interaction in the Tunneling Dynamics of Lanthanide Molecular Magnets. *J. Appl. Phys.* **2019**, *125*, No. 142903.
(32) Thiele, S.; Vincent, R.; Holzmann, M.; Klyatskaya, S.; Ruben, M.; Balestro, F.; Wernsdorfer, W. Electrical Readout of Individual Nuclear Spin Trajectories in a Single-Molecule Magnet Spin Transistor. *Phys. Rev. Lett.* **2013**, *111*, No. 037203.
(33) Godfrin, C.; Thiele, S.; Ferhat, A.; Klyatskaya, S.; Ruben, M.; Wernsdorfer, W.; Balestro, F. Electrical Read-Out of a Single Spin Using an Exchange-Coupled Quantum Dot. *ACS Nano* **2017**, *11*, 3984−3989.
(34) Troiani, F.; Godfrin, C.; Thiele, S.; Balestro, F.; Wernsdorfer, W.; Klyatskaya, S.; Ruben, M.; Affronte, M. Landau-Zener Transition in a Continuously Measured Single-Molecule Spin Transistor. *Phys. Rev. Lett.* **2017**, *118*, No. 257701.
(35) Thiele, S.; Balestro, F.; Ballou, R.; Klyatskaya, S.; Ruben, M.; Wernsdorfer, W. Electrically Driven Nuclear Spin Resonance in Single-Molecule Magnets. *Science* **2014**, *344*, 1135−1138.
(36) Vincent, R.; Klyatskaya, S.; Ruben, M.; Wernsdorfer, W.; Balestro, F. Electronic Read-out of a Single Nuclear Spin Using a Molecular Spin Transistor. *Nature* **2012**, *488*, 357−360.
(37) Ishikawa, N.; Sugita, M.; Ishikawa, T.; Koshihara, S. Y.; Kaizu, Y. Lanthanide Double-Decker Complexes Functioning as Magnets at the Single-Molecular Level. *J. Am. Chem. Soc.* **2003**, *125*, 8694−8695.
(38) Taran, G.; Bonet, E.; Wernsdorfer, W. Decoherence Measurements in Crystals of Molecular Magnets. *Phys. Rev. B* **2019**, *99*, No. 180408.
(39) Urdampilleta, M.; Klyatskaya, S.; Cleuziou, J. P.; Ruben, M.; Wernsdorfer, W. Supramolecular Spin Valves. *Nat. Mater.* **2011**, *10*, 502−506.
(40) Ganzhorn, M.; Klyatskaya, S.; Ruben, M.; Wernsdorfer, W. Quantum Einstein-de Haas Effect. *Nat. Commun.* **2016**, *7*, No. 11443.
(41) Ganzhorn, M.; Klyatskaya, S.; Ruben, M.; Wernsdorfer, W. Strong Spin-Phonon Coupling between a Single-Molecule Magnet and a Carbon Nanotube Nanoelectromechanical System. *Nat. Nanotechnol.* **2013**, *8*, 165−169.
(42) Gatteschi, D.; Sessoli, R.; Villain, J.*Molecular Nanomagnets*; Oxford University Press, 2007; pp 1−408.
(43) Leuenberger, M. N.; Loss, D. Spin Tunneling and Phonon-Assisted Relaxation in Mn12-Acetate. *Phys. Rev. B* **2000**, *61*, 1286−1302.
(44) Lunghi, A.; Sanvito, S. How Do Phonons Relax Molecular Spins? *Sci. Adv.* **2019**, No. eaax7163.
(45) Garlatti, E.; Albino, A.; Chicco, S.; Nguyen, V. H. A.; Santanni, F.; Paolasini, L.; Mazzoli, C.; Caciuffo, R.; Totti, F.; Santini, P.; Sessoli, R.; Lunghi, A.; Carretta, S. The Critical Role of Ultra-Low-Energy Vibrations in the Relaxation Dynamics of Molecular Qubits. *Nat. Commun.* **2023**, *14*, No. 1653.
(46) Garlatti, E.; Tesi, L.; Lunghi, A.; Atzori, M.; Voneshen, D. J.; Santini, P.; Sanvito, S.; Guidi, T.; Sessoli, R.; Carretta, S. Unveiling Phonons in a Molecular Qubit with Four-Dimensional Inelastic Neutron Scattering and Density Functional Theory. *Nat. Commun.* **2020**, *11*, No. 1751.
(47) Granville, S.; Ruck, B. J.; Budde, F.; Trodahl, H. J.; Williams, G. V. M. Nearest-Neighbor Mn Antiferromagnetic Exchange in Ga1-x Mn XN. *Phys. Rev. B* **2010**, *81*, No. 184425.
(48) Moreno-Pineda, E.; Taran, G.; Wernsdorfer, W.; Ruben, M. Quantum Tunnelling of the Magnetisation in Single-Molecule Magnet Isotopologue Dimers. *Chem. Sci.* **2019**, *10*, 5138−5145.